

Abstract We discuss the capability of a third-generation ground-based detector such as the Einstein Telescope (ET) to enhance our astrophysical knowledge through detections of gravitational waves emitted by binaries including intermediate-mass and massive black holes. The design target for such instruments calls for improved sensitivity at low frequencies, specifically in the ~ 1 – 10 Hz range. This will allow the detection of gravitational waves generated in binary systems containing black holes of intermediate mass, ~ 100 – $1000M_{\odot}$. We primarily discuss two different source types — mergers between two intermediate mass black holes (IMBHs) of comparable mass, and intermediate-mass-ratio inspirals (IMRIs) of smaller compact objects with mass ~ 1 – $10M_{\odot}$ into IMBHs. IMBHs may form via two channels: (i) in dark matter halos at high redshift through direct collapse or the collapse of very massive metal-poor Population III stars, or (ii) via runaway stellar collisions in globular clusters. In this paper, we will discuss both formation channels, and both classes of merger in each case. We review existing rate estimates where these exist in the literature, and provide some new calculations for the approximate numbers of events that will be seen by a detector like the Einstein Telescope. These results indicate that the ET may see a few to a few thousand comparable-mass IMBH mergers and as many as several hundred IMRI events per year. These observations will significantly enhance our understanding of galactic black-hole growth, of the existence and properties of IMBHs and of the astrophysics of globular clusters. We finish our review with a discussion of some more speculative sources of gravitational waves for the ET, including hypermassive white dwarfs and eccentric stellar-mass compact-object binaries.

Exploring intermediate and massive black-hole binaries with the Einstein Telescope

Jonathan R. Gair · Ilya Mandel ·
M. Coleman Miller · Marta Volonteri

July 26, 2009

1 Introduction

The Einstein Telescope (ET), a proposed third-generation ground-based gravitational-wave (GW) detector discussed in greater detail elsewhere in this volume, will be able to probe GWs in a frequency range reaching down to ~ 1 Hz [47, 31]. This is lower than the limit of ~ 40 Hz available to current ground-based interferometric GW detectors such as LIGO, Virgo, and GEO-600 or the ~ 10 Hz limit that could be reached by their second generation [94, 2, 40]. On the other hand, GWs in the range above ~ 0.1 Hz will not be accessible to the planned Laser Interferometer Space Antenna (LISA, [12]), which is sensitive to low-frequency radiation. The frequency range determines the typical masses of coalescing binaries that could be detected by an interferometer; for example, the frequency of GWs emitted from the innermost stable circular orbit of a test particle around a Schwarzschild black hole of mass M is $\approx 4400 \text{ Hz}(M_{\odot}/M)$. The Einstein Telescope will therefore probe sources with masses of hundreds or a few thousand M_{\odot} which are out of reach of LISA or the current ground-based detectors. This places the ET in a position to make complementary observations to LISA and LIGO/Virgo/GEO-600 and to carry out unique searches for several very exciting source types, particularly those involving light seeds of massive black holes and intermediate-mass black holes.

J. R. Gair

Institute of Astronomy, University of Cambridge, Cambridge, CB30HA, UK

I. Mandel

Department of Physics and Astronomy, Northwestern University, Evanston, IL, 60208 USA

M. C. Miller

University of Maryland, Department of Astronomy and Center for Theory and Computation, College Park, MD 20742

M. Volonteri

Department of Astronomy, University of Michigan, Ann Arbor, MI 48109

There is a significant body of evidence that massive black holes (MBHs) are generically found in the centers of massive galaxies [26]. These MBHs merge during mergers of their host galaxies, and such mergers therefore trace the history of structure formation in the universe. Gravitational waves emitted during the mergers of MBHs with masses above $1000 M_{\odot}$ will be detectable by LISA; dozens of detections could be made during the LISA mission [91]. According to some predictions, these massive black holes grow from light seeds of $\sim 100 M_{\odot}$ through accretion and mergers [57, 105, 92]. The typical frequencies of gravitational radiation emitted during the mergers of such systems will fall in the 0.1 – 10 Hz range, however, and will only be accessible to GW detectors sensitive in that range. The Einstein Telescope may be able to detect tens of such sources, determining their masses to an accuracy of a few percent and the luminosity distances to $\lesssim 30\%$ [90, 34].

Meanwhile, globular clusters may host intermediate-mass black holes (IMBHs) with masses in the $\sim 100 - 1000 M_{\odot}$ range (see [67, 66] for reviews). Intermediate-mass-ratio inspirals of neutron stars or stellar-mass black holes into these IMBHs could be detected by the second generation of ground-based detectors [62]; however, the Einstein Telescope should be able to detect far greater numbers of events ranging to higher IMBH masses. If the binary fraction in a globular cluster is sufficiently high, an IMBH-IMBH binary can form and then coalesce, emitting gravitational waves in the process [30]. The Einstein Telescope may be able to detect thousands of such events, although, given the present uncertainty about the very existence of IMBHs, all such estimates must be viewed with a great deal of caution.

The Einstein Telescope may also be able to detect a number of other, more speculative sources. These include the inspirals of stellar-mass black holes into IMBHs that may reside at the centers of dwarf galaxies, although we do not expect a significant rate of detectable signals of this type. We also discuss the possibility of detecting orbiting white dwarfs near the upper end of their allowed mass range, and the intriguing prospect of searching for eccentric binaries.

This paper is organized as follows. In Section 2, we discuss the methodology for event-rate and parameter-estimation calculations. We describe the adopted detector and network models, the waveform families used, and the formalism for estimating the signal-to-noise ratio and parameter-estimation accuracy. We then discuss in detail several types of GW sources of particular relevance to the ET. In Section 3, we consider sources involving IMBHs in globular clusters, both intermediate-mass-ratio inspirals and IMBH-IMBH coalescences. In Section 4, we focus on light massive black holes, either as light seeds at high redshift or as central bodies in dwarf galaxies. And in Section 5, we discuss several speculative sources, including hypermassive white dwarfs and eccentric binaries. We end with a discussion and summary in Section 6.

2 Methodology for event-rate and parameter-estimation calculations

2.1 The Einstein Telescope configuration

The design target for the Einstein telescope is a 10km scale interferometer, with a factor of ~ 10 increase in sensitivity over Advanced LIGO, and improved sensitivity at low frequencies. The ET design also calls for the ability to measure polarisation at a single site, which requires at least two non-coaligned coplanar detectors at the site. The currently favoured configuration is a triangular facility, with 10km long arms, and containing three independent detectors with 60° opening angles, as this has lower infrastructure costs and slightly better sensitivity than two right angle detectors placed at 45° to one another [31]. We refer to this triangular design as a “single ET”. In Figure 1 we show the target ET noise curve, labelled “ET baseline” [47]. This noise curve is for a single right-angle interferometer with the ET design sensitivity. Unless otherwise stated, signal-to-noise ratios (SNRs) etc. will be quoted for this configuration. The sensitivities of one 60° interferometer, two right-angle interferometers and a single ET are changed relative to this by factors of $\sqrt{3}/2$, $\sqrt{2}$ and $3/2$ respectively. The “ET baseline” design has recently been superseded by the curve labelled “ET B” in Figure 1, but we have checked that this change does not significantly affect our results, since the noise curves are largely similar in the frequency range where massive systems accumulate most of their SNR. Figure 1 also shows an alternative ‘xylophone’ configuration for ET that was described in [48]. This trades off improved sensitivity near 10Hz for decreased sensitivity at higher frequencies. It has not yet been decided what fraction of the time ET will operate in the baseline, broadband, mode or the xylophone mode. We will see in Figure 3 in Section 4.1 that the xylophone mode is to be preferred for the detection of black hole binaries in the $100\text{--}1000M_\odot$ range.

In Section 4.1 we will discuss parameter estimation for mergers of light seeds of massive black holes detected by ET. As the events are short lived, parameter estimation requires the existence of a network containing multiple detectors. We will discuss the same four third-generation network configurations discussed in [90,34] — (i) one ET at the geographic location of Virgo, plus a second right-angle 10km detector at the location of LIGO Hanford or Perth (Australia); (ii) as configuration (i) plus a third 10km detector at the location of LIGO Livingston; (iii) as configuration (i) but with the Hanford/Perth 10km detector replaced by a second ET; and (iv) three ETs, one at each of the three sites.

2.2 Waveforms

In this paper, we will primarily consider two different types of source — binaries consisting of two intermediate mass black holes of comparable mass; and

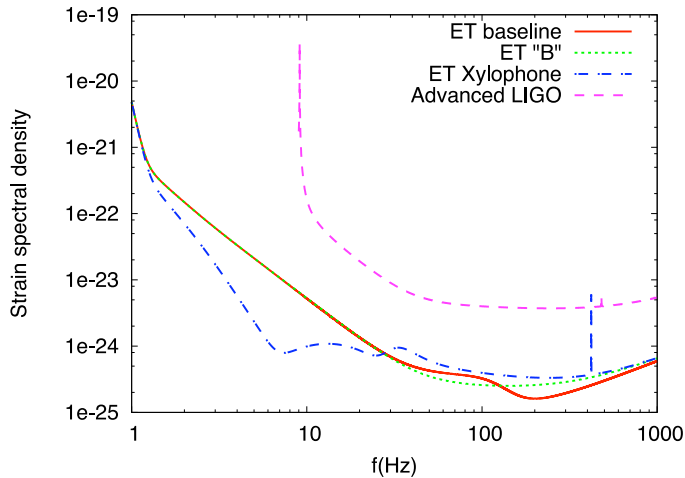


Fig. 1 Sensitivity curve, $\sqrt{S_h(f)}$, for three configurations of the Einstein Telescope, as described in the text. We also show the Advanced LIGO noise curve for reference.

intermediate-mass-ratio inspirals (IMRIs) of a stellar mass compact object (a neutron star or black hole) into an IMBH. We model the gravitational waves emitted by these systems in different ways. For comparable mass binary systems at the upper end of the detectable mass range, a significant amount of energy is radiated during the merger and ringdown phases and so it is important to include these in waveform models for signal-to-noise ratio (SNR) calculation and parameter estimation. The recent advances in numerical relativity have allowed the construction of hybrid waveform models that include inspiral, merger and ringdown in a self-consistent way in a single template. The models use post-Newtonian expressions to model the inspiral radiation, which are matched onto fits to numerical relativity simulations for the merger radiation and then onto analytic expressions for the quasinormal mode ringdown radiation. We use two families of waveforms in the current work — the “phenomenological” inspiral, merger, ringdown model (IMR) [4], and the effective-one-body, numerical relativity (EOBNR) model [19]. The IMR model prescribes the Fourier domain waveform of an optimally-oriented source in the form

$$h(f) \equiv A_{\text{eff}}(f) \exp(i\Psi_{\text{eff}}(f)), \quad A_{\text{eff}} \equiv C \begin{cases} (f/f_{\text{merg}})^{-7/6} & \text{if } f < f_{\text{merg}} \\ (f/f_{\text{merg}})^{-2/3} & \text{if } f_{\text{merg}} \leq f < f_{\text{ring}} \\ w\mathcal{L}(f, f_{\text{ring}}, \sigma) & \text{if } f_{\text{ring}} \leq f < f_{\text{cut}} \end{cases} \quad (1)$$

Expressions for f_{merg} , f_{ring} , f_{cut} , $\Psi_{\text{eff}}(f)$, C , w and $\mathcal{L}(f, f_{\text{ring}}, \sigma)$ are given in Eqs. (4.14)-(4.19) and Tables I-II of [4] (updated coefficients are available [3], but yield nearly identical SNRs [34]). We denote the mass of the most massive object in the binary by m_1 and the less massive object by m_2 . The IMR waveforms depend on the total mass of the binary, $M = m_1 + m_2$, the

reduced mass ratio, $\eta = m_1 m_2 / M^2$ and the time of merger, t_0 . Including the detector response introduces six additional extrinsic parameters expressing the relative location and orientation of the source and detector: the distance, the two sky-location angles, two binary orientation angles, and the phase at some fiducial time, e.g., t_0 . The EOBNR waveforms are conceptually similar; however, they are based on the analytical effective-one-body formalism and designed to match perturbative results in the limit $\eta \rightarrow 0$.

The SNRs of typical ET events computed using these two waveform families agree to $\sim 20\%$ [34], with the IMR predictions being higher for low mass ratios, $\eta \approx 0.16$, and the EOBNR predictions being higher for high mass ratios, $\eta \approx 0.25$. The similarity between these results provides confidence that the estimates are approximately correct, while the difference provides an indication of the uncertainty in the SNR calculations. A $\sim 20\%$ SNR uncertainty is small compared to the uncertainty in the astrophysics for IMBH sources. Recent comparisons with numerical data suggest that errors in EOBNR waveforms are significantly smaller, at least for equal-mass sources [20]; meanwhile, IMR waveforms are also undergoing significant improvements.

The IMR and EOBNR waveforms have been matched to numerical relativity simulations, but only for mass ratios of 1:4 and higher. Computational requirements suggest it is unlikely that numerical simulations using current techniques will go beyond mass ratios of $\sim 1:10$ in the near future, although this may be possible using innovative new approaches. Post-Newtonian theory also breaks down once the mass-ratio becomes too extreme. For very extreme mass ratios, $\eta \sim 10^{-6}$ – 10^{-4} , gravitational waveforms can be computed using black hole perturbation theory [79], in which the smaller object is regarded as a perturbing field of the background spacetime of the larger object and radiation reaction is described in terms of the ‘self-force’. Significant progress has been made over the past few years in self-force calculations, which have led to the calculation of the self-force for circular orbits in the Schwarzschild spacetime [7], including the shift in the location of the innermost-stable-circular-orbit (ISCO) that results from the action of this force [8]. However, even at mass ratios of $\sim 10^{-5}$, the terms that are missing in the first-order self-force formalism are estimated to have a marginal effect in the phasing of waveforms for LISA sources [52]. The mass ratios for typical IMRI sources for ET lie somewhere between these extremes, being typically ~ 0.001 – 0.1 . In this regime neither post-Newtonian nor perturbative waveforms will be adequate on their own to model the true waveforms [63]. More research is needed to devise waveforms that are suitable for filling this gap. In the meantime we have made do with available waveforms, with the understanding that these will not be completely accurate.

We have estimated IMRI SNRs using the EOBNR waveforms, which will be accurate for $\eta \approx 1$ and are designed to be approximately correct in the limit $\eta \rightarrow 0$. For comparison, we have also computed SNRs for the inspiral phase only using perturbative waveforms for circular and equatorial inspirals, as described and tabulated in [29], and as used to estimate SNRs for LISA in [33], as well as with the IMR waveforms described earlier. For the early

portion of the inspiral, significantly before the last stable orbit, we find that the SNRs obtained with the three waveform families agree to within $\sim 10\%$; this difference is of a comparable magnitude to the effect of omitting relativistic corrections to post-Newtonian inspirals. We find, however, that for the more massive systems, when merger and ringdown contribute a significant portion of the SNR, estimates from the IMR and EOBNR waveforms differ very significantly, with IMR waveforms predicting SNRs that are greater by more than an order of magnitude. We see, however, that contrary to theoretical expectations which suggest that the energy emitted during the ringdown should scale as $\eta^2 \times M$, so that the SNR should scale as η for a fixed total mass, the SNR predicted by the ringdown portion of the IMR waveform scales roughly as $\sqrt{\eta}$. We therefore use EOBNR waveforms, which exhibit the correct scaling, for estimating IMRI SNRs with the understanding that there is a clear need for more careful and accurate modelling of IMRI radiation in the future, not least because detection of these systems will almost certainly rely on matched filtering, for which accurate template waveforms are a necessity.

2.3 Signal-to-noise ratio and parameter estimation

The signal-to-noise ratio (SNR) ρ for a waveform $h(t)$ measured by a single detector with one-sided noise power spectral density $S_n(|f|)$ is given by $\rho^2 = \langle h|h \rangle$. Here $\langle a|b \rangle$ is the noise-weighted inner product

$$\langle a|b \rangle \equiv 4\Re \int_0^\infty \frac{\tilde{a}(f)\tilde{b}(f)^*}{S_n(|f|)} df, \quad (2)$$

where $\tilde{a}(f)$ is the Fourier transform of the waveform $a(t)$ and $*$ denotes the complex conjugate.

We define the horizon distance D_{hor} as the distance at which a detector can detect a waveform from an optimally oriented, overhead source at an SNR threshold of 8. The actual gravitational-wave emission is not isotropic. We define the average range as the radius of a sphere whose volume is equal to the volume in which inspiral sources can be detected at an SNR threshold of 8. For uniformly located, randomly oriented sources, and without applying corrections for cosmological redshift, the range is related to the horizon distance by $D = D_{\text{hor}}/2.26$ [28]. In this paper, we will apply the same correction factor even when the source distribution is redshift dependent and when the cosmological redshift is important; more rigorous calculations may be useful in the future.

To determine the accuracy of parameter estimation, we employ a formalism based on the Fisher information matrix,

$$\Gamma_{ij} = \left\langle \frac{\partial h}{\partial \theta_i} \middle| \frac{\partial h}{\partial \theta_j} \right\rangle, \quad (3)$$

where $\boldsymbol{\theta}$ is the vector of model parameters. However, the Fisher-matrix approach can over-predict the accuracy of parameter estimation when SNRs

are low and the parameter space has multiple islands with nearly degenerate waveforms [100]. In addition to these statistical errors, systematic errors in parameter determination can be caused by imperfect knowledge of the waveform used for parameter estimation [23], or by failing to include salient features such as spin in the waveform templates [102].

For multiple detectors, the inner products in equations (2) and (3) should be replaced by sums of inner products over individual detectors. Thus, the existence of N identical interferometers will increase the range by a factor of \sqrt{N} over the single-interferometer range if the network SNR threshold is fixed.

3 IMBH sources in Globular Clusters

A particularly exciting possibility for GW astronomy involves intermediate-mass black holes (IMBHs) in globular clusters. Observational evidence from cluster dynamics and from ultraluminous X-ray sources suggests that there may exist a population of intermediate-mass black holes (IMBHs) with masses of $M \sim 10^2 - 10^4 M_\odot$ [67, 99, 74]. The lack of definitive dynamical evidence for IMBHs means, however, that their existence is still inconclusive and alternate explanations have been proposed (see [53, 13] for recent discussions).

If IMBHs exist, they could form through runaway collisions of massive stars on time scales too short to allow for stellar evolution, $\lesssim 3$ Myr [80]. More recent simulations of runaway collisions with the inclusion of stellar winds suggest that winds will prevent the growth of IMBHs in all but the most metal-poor environments [37], although these simulations extrapolate wind rates from much less massive stars and the collision rates are likely to mean that the collision products will be extended bags of gas rather than relaxed stars. Alternatively, IMBHs could form through mergers of stellar-mass black holes in dense subclusters at the cores of globular clusters; however, recoil kicks may eject the products of such collisions from the host globulars [76]. We refer the reader to [67, 66] for reviews.

Numerical simulations of globular clusters suggest that IMBHs could merge with numerous lower-mass compact objects (COs) during the lifetime of the cluster [98, 69, 68, 72, 71, 41, 42, 76, 62], through a combination of the emission of gravitational radiation, binary exchange processes, and secular evolution of hierarchical triple systems. For IMBH mass $\lesssim 3000 M_\odot$, the GWs generated during the inspiral of a stellar-mass object (black hole or neutron star, since a white dwarf or a main sequence star would be tidally disrupted) into an IMBH are potentially detectable by the Einstein Telescope. Ringdown radiation could be detected for even more massive IMBHs.

When the primordial binary fraction in a globular cluster is sufficiently high, $\gtrsim 10\%$, stellar collisions during binary scattering interactions may lead to the production of two IMBHs in a single cluster [43]. Since observations and numerical calculations suggest that clusters may be born with large binary fractions (e.g., [54]), the formation of two IMBHs may be generic in sufficiently dense and massive clusters. If this happens, the two IMBHs will

exchange into a common binary which, after shrinking via dynamical friction and dynamical encounters with other stars, will merge through radiation reaction; all of these processes occur on a timescale of $\lesssim 10$ Myr [30]. [There may also be a possibility that two IMBHs from different globular clusters merge during the merger of their parent clusters [5]; we do not discuss this channel here.]

In the following two subsections, we estimate the rates with which the Einstein Telescope could detect gravitational waves from the inspirals of stellar-mass compact-objects into an IMBH and the coalescence of an IMBH-IMBH binaries.

3.1 Intermediate-mass-ratio inspirals into IMBHs

In an earlier work, a subset of the authors analyzed the possibility of detecting intermediate-mass-ratio inspirals (IMRIs) of compact objects into IMBHs with Advanced LIGO [62]. There, we found that the binary tightening via three-body interactions was the dominant formation scenario for IMRIs. The IMBH, as the most massive object in the cluster, readily switches into compact-object (CO) binaries. Once a sufficiently hard CO-IMBH binary is formed, the binary will be hardened rather than disrupted by three-body interactions with other stars from the cluster. Eventually, as the interacting stars take away energy from the binary, the binary will tighten to the point where radiation reaction from gravitational-wave emission will drive the binary to coalesce. For neutron-star or black-hole COs, we can compute the distance to which the gravitational waves can be detected and convert it into detection rates.

Here, we repeat that calculation for ET sources, with the following two major changes. First, we take advantage of the recent development of hybrid waveforms that describe all three phases of the coalescence – inspiral, merger, and ringdown – to compute the SNR from the full GW signal, rather than just the inspiral portion. As described in Section 2.2, we apply EOBNR waveforms [19] to this calculation, while recognizing that they have not been tested for intermediate mass ratios. Second, because ET has a lower frequency cutoff ~ 1 Hz than Advanced LIGO (~ 10 Hz), we consider inspirals into $1000M_\odot$ IMBHs along with inspirals into $100M_\odot$ IMBHs. We note, however, that for higher IMBH masses, the IMBH could dominate the dynamics in the center of the cluster and a cusp could be formed around the IMBH, possibly increasing the importance of the direct-capture scenario [51]; additional discussion of this possibility can be found in Section 2.3 of [62].

Approximately $(2\pi/22)M/m_*$ close interactions with stars of mass m_* are required to reduce the semimajor axis of the CO-IMBH binary with IMBH mass M by one e -folding [84]. Stars come within the semimajor axis separation a from the binary at a rate of

$$\dot{N} \approx n \left[\pi a \frac{2GM}{\sigma^2} \right] \sigma = 3 \times 10^{-7} \frac{n}{10^{5.5} \text{ pc}^{-3}} \frac{a}{10^{13} \text{ cm}} \frac{M}{100M_\odot} \frac{10 \text{ km/s}}{\sigma} \text{ yr}^{-1}, \quad (4)$$

where n is the number density of stars in a globular cluster, the bracketed expression is the gravitationally focused cross-section, and σ is the velocity dispersion. The last e -folding time dominates the hardening rate, so the hardening time-scale is

$$T_{\text{harden}} \approx \frac{2\pi}{22} \frac{M}{m_*} \frac{1}{N} \approx 2 \times 10^8 \frac{10^{5.5} \text{ pc}^{-3} 10^{13} \text{ cm}}{n} \frac{\sigma}{10 \text{ km/s}} \frac{0.5 M_\odot}{m_*} \text{ yr}. \quad (5)$$

Meanwhile, the timescale for the binary of semimajor axis a , eccentricity e , reduced mass approximately equal to the CO mass $\mu \approx m$, and total mass $\approx M$ is [78]

$$T_{\text{merge}} \approx 10^{17} \frac{M_\odot^3}{M^2 m} \left(\frac{a}{10^{13} \text{ cm}} \right)^4 (1-e^2)^{7/2} \text{ yr} \approx 10^8 \frac{M_\odot}{m} \left(\frac{100 M_\odot}{M} \right)^2 \left(\frac{a}{10^{13} \text{ cm}} \right)^4 \text{ yr}, \quad (6)$$

where in the last equality we set $e \approx 0.98$ as the eccentricity after the final three-body encounter, following [42]. Minimizing the total merger time $T = T_{\text{harden}} + T_{\text{merge}}$ over a while setting n , v and m_* to their fiducial values allows us to compute the CO-IMBH coalescence rate per globular cluster, $1/T$.

To compute the range at which the Einstein Telescope can detect such IMRIs, we follow the procedure outlined in Section 2.3. We use EOBNR waveforms and ignore the spin of the IMBH, which we expect to be small, $S/M^2 \lesssim 0.3$, after a significant number of minor mergers [61]. We compute the horizon distance for a “single ET” configuration, and divide it by 2.26 to obtain the typical range D [28], although this procedure does not correctly average over sky-location and orientation angles when redshift is important. The range is a function of the redshifted masses of the IMBH $M_z = M(1+z)$ and the compact object $m_z = m(1+z)$. After computing the range, we convert it into a redshift by inverting the following expression for the luminosity distance as a function of redshift [50]:

$$D_L(z) = D_H(1+z) \left\{ \int_0^z \frac{dz'}{[\Omega_M(1+z')^3 + \Omega_\Lambda]^{1/2}} \right\}. \quad (7)$$

Here, we implicitly assume a flat universe ($\Omega_k = 0$), and use $\Omega_M = 0.27$, $\Omega_\Lambda = 0.73$, $H_0 = 72 \text{ km s}^{-1} \text{ Mpc}^{-1}$; and $D_H = c/H_0 \approx 4170 \text{ Mpc}$. We assume that the typical source is located near the redshift z that corresponds to the search range, and obtain the source-frame masses by dividing the redshifted masses by $1+z$; we use these source-frame masses to compute the merger timescale T .

We additionally assume that 10% of clusters form an IMBH and are sufficiently dense to be relevant to the rate calculation, and that globular clusters have a fixed comoving space density of $8.4 h^3 \text{ Mpc}^{-3}$ [81]. For $h = 0.72$, this yields a density of $\sim 0.3 \text{ Mpc}^{-3}$ for relevant clusters. We compute the comoving volume up to redshift z by integrating up to z the following expression for

dV_c/dz [50], with the cosmological parameters defined above:

$$\frac{dV_c}{dz} = 4\pi D_H^3 [\Omega_M(1+z)^3 + \Omega_\Lambda]^{-1/2} \left\{ \int_0^z \frac{dz'}{[\Omega_M(1+z')^3 + \Omega_\Lambda]^{1/2}} \right\}^2. \quad (8)$$

Therefore, the event rate is given by $\sim 0.3(V_c/\text{Mpc})^3/T$.

M_z/M_\odot	m_z/M_\odot	D/Gpc	z	M/M_\odot	m/M_\odot	T/yr	V_c/Mpc^3	Events/yr
100	10	11	1.5	40	4	3×10^8	3×10^{11}	300
100	2	4.9	0.8	56	1.1	4×10^8	5×10^{11}	70
1000	10	3.2	0.6	640	6.4	9×10^7	1.4×10^{11}	120
1000	2	1	0.2	830	1.7	1×10^8	2×10^9	6

Table 1 “Single ET” average range, corresponding redshift, source-frame masses, merger timescale, comoving volume within range, and detectable event rate for several combinations of plausible redshifted CO and IMBH masses.

Table 1 summarizes the rate predictions for four combinations of M_z and m_z . Although the lack of knowledge about IMBHs and their mass distributions makes it impossible to generate firm predictions, it appears that ET may detect up to a thousand compact-object IMRIs into IMBHs during a three-year mission lifetime. Operating in the xylophone configuration would increase these rates further.

3.2 IMBH-IMBH inspirals

We can estimate the rate at which IMBH-IMBH mergers will be detected with the Einstein Telescope following the event rate calculation for LISA and Advanced LIGO described in [30]. Once a pair of IMBHs is formed in a single cluster, they sink rapidly to the center where they form a binary and merge via three-body interactions with the stars in the cluster (see [30, 6] for more details). Therefore, the rate of IMBH binary mergers is just the rate at which pairs of IMBHs form in clusters. The rate of detectable coalescences is

$$R \equiv \frac{dN_{\text{event}}}{dt_o} = \int_{M_{\text{tot}, \text{min}}}^{M_{\text{tot}, \text{max}}} dM_{\text{tot}} \int_0^1 dq \int_0^{z_{\text{max}}(M_{\text{tot}}, q)} dz \frac{d^4 N_{\text{event}}}{dM_{\text{tot}} dq dt_e dV_c} \frac{dt_e}{dt_o} \frac{dV_c}{dz}. \quad (9)$$

Here t_o is the time measured in our observer’s frame and t_e is the time measured at the redshift z of the merger; M_{tot} is the total mass of the coalescing IMBH-IMBH binary and $q \leq 1$ is the mass ratio between the IMBHs; $z_{\text{max}}(M_{\text{tot}}, q)$ is the maximum redshift to which the ET could detect a merger between two IMBHs of total mass M_{tot} and mass ratio q ; $dt_e/dt_o = (1+z)^{-1}$ is the relation between local time and our observed time, and dV_c/dz is the change of comoving volume with redshift, given by Eq. (8).

We make the following assumptions:

- IMBH pairs form in a fraction g of all globular clusters.
- We neglect the delay between cluster formation and IMBH coalescence.
- When an IMBH pair forms in a cluster, its total mass is a fixed fraction of the cluster mass, $M_{\text{tot}} = 2 \times 10^{-3} M_{\text{cl}}$, consistent with simulations [44]. The mass ratio is uniformly distributed between 0 and 1. We restrict our attention to systems with a total mass between $M_{\text{tot},\text{min}} = 100M_{\odot}$ and $M_{\text{tot},\text{max}} = 20000M_{\odot}$. i.e., $5 \times 10^4 \leq M_{\text{cl}}/M_{\odot} \leq 10^7$. Thus,

$$\frac{d^4 N_{\text{event}}}{dM_{\text{tot}} dq dt_e dV_c} = g \frac{d^3 N_{\text{cl}}}{dM_{\text{cl}} dt_e dV_c} \frac{1}{2 \times 10^{-3}}. \quad (10)$$

- The distribution of cluster masses scales as $(dN_{\text{cl}}/dM_{\text{cl}}) \propto M_{\text{cl}}^{-2}$ independently of redshift. We confine our attention to clusters with masses ranging from $M_{\text{cl},\text{min}} = 5 \times 10^4 M_{\odot}$ to $M_{\text{cl},\text{max}} = 10^7 M_{\odot}$ (note that the lower limit is different from that chosen in [30] since here we set $M_{\text{tot},\text{min}} = 100M_{\odot}$ for IMBH sources). The total mass formed in all clusters in this mass range at a given redshift is a redshift-independent fraction g_{cl} of the total star formation rate per comoving volume:

$$g_{\text{cl}} \frac{d^2 M_{\text{SF}}}{dV_c dt_e} = \int_{M_{\text{cl},\text{min}}}^{M_{\text{cl},\text{max}}} \frac{d^3 N_{\text{cl}}}{dM_{\text{cl}} dt_e dV_c} M_{\text{cl}} dM_{\text{cl}}, \quad (11)$$

which provides the normalization for $dN_{\text{cl}}/dM_{\text{cl}}$:

$$\frac{d^3 N_{\text{cl}}}{dM_{\text{cl}} dt_e dV_c} = \frac{g_{\text{cl}}}{\ln(M_{\text{cl},\text{max}}/M_{\text{cl},\text{min}})} \frac{d^2 M_{\text{SF}}}{dV_c dt_e} \frac{1}{M_{\text{cl}}^2}. \quad (12)$$

- The star formation rate as a function of redshift z is

$$\frac{d^2 M_{\text{SF}}}{dV_c dt_e} = 0.17 \frac{e^{3.4z}}{e^{3.4z} + 22} \frac{[\Omega_M(1+z)^3 + \Omega_A]^{1/2}}{(1+z)^{3/2}} M_{\odot} \text{ yr}^{-1} \text{ Mpc}^{-3}. \quad (13)$$

This is the formula used by [97], in which the star formation rate rises rapidly with increasing z to $z \sim 2$, after which it remains roughly constant. As in Section 3.1, we assume a flat universe ($\Omega_k = 0$), and use $\Omega_M = 0.27$, $\Omega_A = 0.73$, and $H_0 = 72 \text{ km s}^{-1} \text{ Mpc}^{-1}$.

Substituting these expressions into Eq. (9), the rate of detectable coalescences per year is given by

$$R = \frac{2 \times 10^{-3} g g_{\text{cl}}}{\ln(M_{\text{tot},\text{max}}/M_{\text{tot},\text{min}})} \int_{M_{\text{tot},\text{min}}}^{M_{\text{tot},\text{max}}} \frac{dM_{\text{tot}}}{M_{\text{tot}}^2} \int_0^1 dq \quad (14)$$

$$\int_0^{z_{\text{max}}(M_{\text{tot}},q)} dz \, 0.17 \frac{e^{3.4z}}{e^{3.4z} + 22} \frac{4\pi D_H^3}{(1+z)^{5/2}} \times \left\{ \int_0^z \frac{dz'}{[\Omega_M(1+z')^3 + \Omega_A]^{1/2}} \right\}^2.$$

Note that here M_{tot} is measured in solar masses and D_H is measured in Mpc.

Rather than computing $z_{\max}(M_{\text{tot}}, q)$ for all values of M_{tot} and q , we rely on the following fitting formula for the luminosity-distance range $D_{\text{L,max}}$ as a function of the redshifted total mass $M_z = M_{\text{tot}}(1+z)$, obtained by using EOBNR waveforms to model the coalescence:

$$D_{\text{L,max}}(M_z) = (1.25 \text{ Gpc})A \begin{cases} M_z^{3/5} & \text{if } M_z < M_0 \\ M_z^{11/10} M_z^{-1/2} & \text{if } M_z > M_0 \end{cases}, \quad (15)$$

where $A = 4$, $M_0 = 600M_\odot$ for $q = 1$ and $A = 2.25$, $M_0 = 450M_\odot$ for $q = 0.25$. We use $\rho = 8$ as the SNR threshold for a ‘‘single ET’’ configuration. We also approximate averaging over source sky-location angles and orientations by a factor of $1/2.26$, even though this conversion factor between the horizon distance and the average range is only applicable when the source distribution is isotropic and redshift corrections are unimportant (see Section 2.3).

We can compute $z(D_L)$ by inverting Eq. (7). For a given choice of M_{tot} and q , the maximum detectable redshift $z_{\max}(M_{\text{tot}}, q)$ is then obtained by finding a self-consistent solution of

$$z\left(D_{\text{L,max}}\left(M_{\text{tot}}(1+z_{\max})\right)\right) = z_{\max}. \quad (16)$$

We carry out the integrals of M_{tot} and z in Eq. (14) for two specific values of q . For $q = 1$, we find the total rate to be $R = 2.5 \times 10^5 g g_{\text{cl}}$; for $q = 0.25$, it is $R = 2 \times 10^5 g g_{\text{cl}}$. The range varies smoothly with q ; therefore, we estimate that the full rate, including the integral over q is

$$R \approx 2000 \left(\frac{g}{0.1}\right) \left(\frac{g_{\text{cl}}}{0.1}\right) \text{yr}^{-1}, \quad (17)$$

where we arbitrarily chose $g = 0.1$ and $g_{\text{cl}} = 0.1$ as the default scales for these unknown parameters.

4 Sources in low-mass galaxies

4.1 Light seeds of MBHs at high redshifts

Supermassive black holes (SMBHs) weighing millions to billions of solar masses are nowadays believed to reside in most local galaxies [26, and references therein]. The masses of today’s SMBHs exhibit clear correlations with the properties of their host galaxies (luminosity, mass, and stellar velocity dispersion), suggesting there is a single mechanism for assembling SMBHs and forming galaxies. The evidence therefore favours a co-evolution between galaxies and SMBHs.

In the currently favoured cold dark matter cosmology, galaxies today are expected to have been built up, via a series of mergers, from small-mass building blocks that condensed out at early cosmic times. A single big galaxy can be traced back to hundreds of smaller components with individual masses as low as $\sim 10^5 M_\odot$. Similarly, we expect the SMBHs found in galaxies today to

have grown partially by accretion and partially by mergers following mergers between galaxies (e.g., [105,60]), so that a single SMBH can be traced back to some number of ‘seed’ black holes at early times [106]. There are large uncertainties in this picture, however. Did seed black holes form efficiently in small galaxies (with shallow potential wells) at early times, or was their formation delayed until substantial galaxies with deeper potential wells had been formed? This is a key question, as the mass and the occupation number of the seeds ultimately dictates the occupation number of SMBHs in galactic centers.

The formation of SMBHs is far less well understood than that of their light stellar-mass counterparts. The ‘flow chart’ presented by [86] still stands as a guideline for the possible paths leading to the formation of SMBH seeds in galactic nuclei. One possibility is that the seeds of SMBHs were the remnants of the first generation of stars, formed out of zero-metallicity gas [57]. In a cold dark matter universe, structure builds up hierarchically, so the smaller clumps at the earliest cosmic times have shallower potential wells. Stars cannot form until the clumps are sufficiently big to provide a potential well deep enough to pull in gas that can cool radiatively and contract to make a protostar. This requires dark matter clumps – minihalos – of $\sim 10^6 M_\odot$ at redshifts of $z \sim 20$. The first stars forming in these minihalos develop under very different conditions from present-day stars: there are no heavy elements (so that molecular hydrogen is the only effective coolant), no dust, and no magnetic fields. These conditions mean that these ‘Population III’ stars were likely very massive, having characteristic masses of the order of $\sim 100 M_\odot$ (e.g., [16, 73, 1, 111]). This prediction relies on the absence of efficient cooling agents in the primordial metal-free gas. If Population III stars form with masses $40 M_\odot < M < 140 M_\odot$ or $M > 260 M_\odot$, they are predicted to collapse and form IMBHs directly with little mass loss [32], i.e., leaving behind seed IMBHs with masses $M_{BH} \sim 10^2 - 10^3 M_\odot$. This is a plausible formation mechanism for the seeds upon which supermassive black holes are grown [105], although more massive black holes may have been formed after the epoch of the first stars in dark-matter halos with virial temperatures of $\sim 10^4$ K [17, 95, 11].

As described in Section 3.1, the formation of an IMBH as a result of dynamical interactions in dense stellar systems is a long-standing idea. This process could have been very effective in the very first stellar clusters that formed in high-redshift proto-galaxies, when the Universe was not as metal-rich as now. Low metallicity favors the growth of a very massive star, the precursor of an IMBH remnant. The mass loss due to winds is significantly reduced in metal-poor stars, which greatly helps in increasing the mass of the final IMBH remnant (cf. [112]). The formation of stellar clusters and the possible evolution of the stellar systems up to IMBH formation are explored in [24]. Figure 2 shows three mass functions for three different MBH ‘seed’ scenarios: direct collapse [11], runaway stellar mergers in high-redshift clusters, and Population III remnants [105].

It is uncertain how many MBH ‘seeds’ formed, and in which mass range. Equally uncertain is how these ‘seed’ black holes grew within their host minihalos. It is not obvious if efficient accretion onto these seeds could have taken

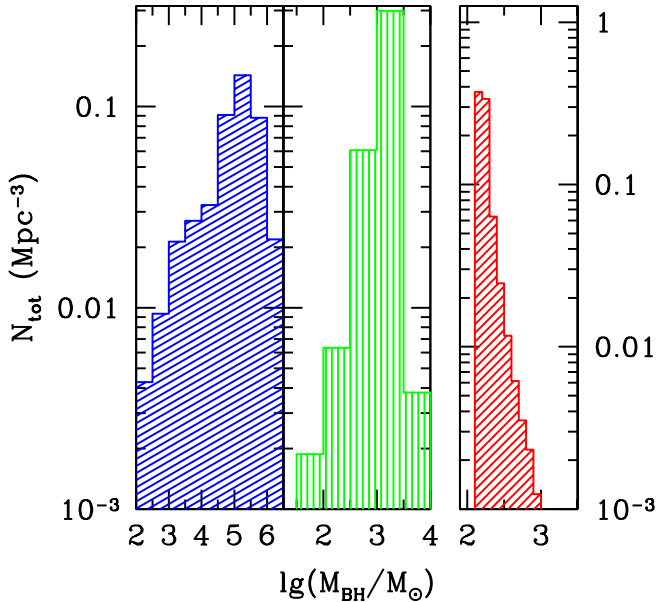


Fig. 2 Mass function of seed MBHs for three different formation scenarios: direct collapse [106, left], runaway stellar mergers in high-redshift clusters [24, center], and Population III remnants [57, right]. Note the different y-axis scale for the Population III case.

place, at least early on, in the fragile environment that the shallow potential wells of minihalos represent [70]. It is likely that seed IMBHs can grow efficiently only if they are hosted in the most massive galaxies at these early cosmic epochs, while IMBHs in an ‘average’ galaxy could have experienced intermittent and inefficient accretion, thus leaving behind a population of underfed IMBHs with a mass range similar to that of the original seeds, $M_{BH} \sim 10^2 - 10^3 M_{\odot}$.

The Einstein Telescope will be able to probe mergers between black-hole seeds at high redshift, and thus help to distinguish between the light-seed model described here, and alternative ‘heavy-seed’ models in which seeds have masses $\sim 10^5 M_{\odot}$ [17]. An estimate for the ET event rate can be computed using Monte-Carlo merger-tree realizations based on the extended Press-Schechter formalism [82], as described in [105,107]. This was done in [90], where four different models were considered that were based on the same merger tree realisations (taken from [105,107]), but differed in the initial mass distribution of seeds and in the prescription for accretion onto the seed black holes. In these scenarios, which were all based on having light, Pop III remnants as the seeds for black hole formation (see discussion earlier in this section), a single ET would detect $\sim 1-10$ seed mergers, depending on the model. The

detected mergers would be between black holes with total mass ranging from $2M_{\min}$ up to $\sim 1000M_{\odot}$, where M_{\min} is the mass of the lightest seed black hole in the initial mass distribution. This minimum seed mass is rather uncertain and depends on the details of the model used, as we discussed earlier. In the scenarios considered in [90], M_{\min} was either $10M_{\odot}$ or $150M_{\odot}$. The detected events would be seen at redshifts $z \sim 1-7$, although this could extend to $z \sim 12$ for the lightest seed model, which had $M_{\min} = 10M_{\odot}$. If ET was operated in the xylophone configuration described in Section 2.1, the number of events seen would be increased to several tens, and these would be out to a redshift $z \sim 15$ [34].

Figure 3, reproduced from the data in [34], shows how the number of events seen by ET over three years varies as a function of the signal-to-noise ratio required in a single 10km right-angle interferometer for detection. The SNR required is likely to be ~ 8 for the network of detectors, although this depends somewhat on data-analysis issues, and on the amount of source confusion present in the data stream. A network SNR of 8 corresponds to an SNR in the single right-angle detector of 5.3 for a single ET, or SNRs of 4.8, 3.9, 3.8 and 3.1 for the network configurations (i) – (iv) described in Section 2.1. In Figure 3 we show results for two of the four light-seed models considered in [90], and for both the baseline and xylophone configurations of the detector. The rate for the baseline ET configuration is rather sensitive to the SNR that is ultimately required for a confident detection, but the xylophone configuration is more robust, as it has improved sensitivity at just the right frequency for systems with mass in the $100-1000M_{\odot}$ range. The mergers seen by ET will be complementary to mergers between heavier black holes that will be seen by space-based detectors such as LISA, ALIA or DECIGO [34]. The combination of detectors will provide a nearly complete survey of mergers between galactic black holes, yielding important constraints on astrophysical models of galaxy formation and growth.

One important question is whether ET will be able to distinguish between black-hole mergers coming from this channel, and those described in Section 3.2 that come from globular clusters. To provide constraints on merger histories, it is necessary to know that an observed event is associated with a galaxy merger. The masses and redshifts of events will provide some information, but more work is required to understand what observational signatures provide the best discriminating power. We would expect mergers between seed black holes to occur over a range of redshifts, with some events at redshifts $z \gtrsim 10$. In the mechanism described in Section 3.2, the black-hole binaries form and merge very quickly, so this could also produce events over a range of redshifts. However, the distinction between these two formation channels becomes increasingly vague at high redshift, when galaxies are in the process of formation. What is important for the light-seed scenario is that black holes of low mass, $\sim 100M_{\odot}$, exist at high redshift. Therefore, being able to identify an event as being between two $\sim 100M_{\odot}$ black holes at redshift $z \gtrsim 5$ would be an important constraint, regardless of how that seed had initially formed. A single ET cannot measure the six extrinsic parameters of a merger source

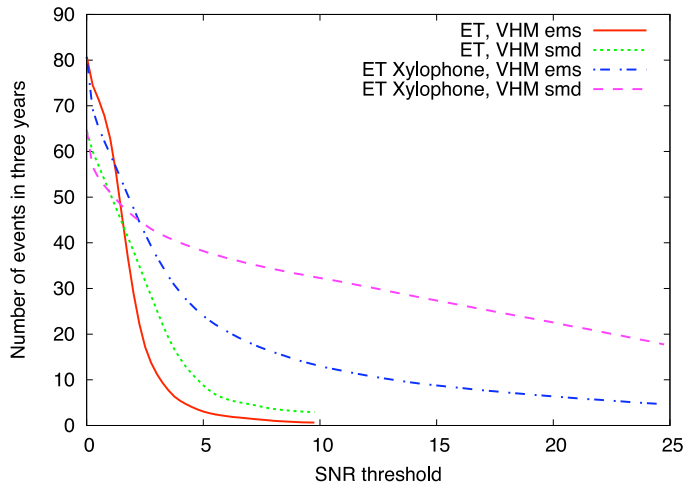


Fig. 3 Number of events detected by the Einstein Telescope in three years, as a function of the required signal-to-noise ratio threshold in a single right-angle detector. Results are shown for both the baseline and xylophone configurations of the Einstein Telescope, and for two different astrophysical models — Volonteri-Hardt-Madau (VHM) with equal mass seeds (*VHM,ems* and VHM with a seed mass distribution (*VHM,smd*). Details on these models can be found in [34].

on its own — at least one additional non-colocated detector will be required. Possible network configurations were discussed in Section 2.1. With one additional 10km detector at the location of LIGO Hanford, the ET network will be able to determine the luminosity distance of a source to an accuracy of $\sim 40\%$. Adding a third 10km detector at the site of LIGO Livingston or upgrading the detectors to ETs improves this modestly to $\sim 30\%$ [90,34]. If we assume that the luminosity distance is converted into a redshift using the concordance cosmology at that time, the redshift error will be comparable to the distance error. Thus, an ET network should be able to say with confidence if an event is indeed occurring between two $\sim 100M_{\odot}$ black holes at high redshift $z \sim 5$.

4.2 MBHs in dwarf galaxies

There are two simple arguments that lead us to believe that $\sim 10^2\text{--}10^3 M_{\odot}$ black holes might inhabit the nuclei of dwarf galaxies today. Firstly, the mass of SMBHs detected in neighboring galaxies scales with the bulge mass — or stellar velocity dispersion ($M_{\text{BH}} - \sigma$) — of their host galaxy [58,35,27,46]. The lowest-mass galaxies currently known have velocity dispersions $\sigma \sim 10\text{--}20 \text{ km s}^{-1}$ [108]. If we extrapolate the $M_{\text{BH}} - \sigma$ correlation to these σ values, we expect the putative IMBHs to have masses in the range of hundreds to thousands of solar masses.

Secondly, as SMBHs grow from lower-mass seeds, it is natural to expect that a leftover population of progenitor IMBHs should also exist in the present

universe. Indeed, one of the best diagnostics of ‘seed’ formation mechanisms would be to measure the masses of IMBHs in dwarf galaxies. This can be understood in terms of the cosmological bias. The progenitors of massive galaxies have a high probability that the central SMBH is not “pristine”, that is, it has increased its mass by accretion, or it has experienced mergers and dynamical interactions. Any dependence of M_{BH} on the initial seed mass is largely erased. However, low-mass galaxies undergo a quieter merger history, and as a result, at low masses the BH occupation fraction and the distribution of BH masses still retain some “memory” of the original seed mass distribution. The signature of the efficiency of the formation of SMBH seeds will consequently be stronger in isolated dwarf galaxies [106].

The record for the smallest known MBH mass belongs to the dwarf Seyfert 1 galaxy POX 52. It is believed to contain a BH of mass $M_{\text{BH}} \sim 10^5 M_{\odot}$ [10]. There are also significant non-detections of BHs in a few nearby galaxies from stellar-dynamical observations, most notably the Local Group Scd-type spiral galaxy M33, in which the upper limit to M_{BH} is just a few thousand solar masses [36,65]. Similarly, in the Local Group dwarf elliptical galaxy NGC 205, $M_{\text{BH}} < 3.8 \times 10^4 M_{\odot}$ [101]. These results suggest that the SMBH “occupation fraction” in low-mass galaxies might be significantly below unity, but at present it is not possible to carry out measurements of similar sensitivity for galaxies much beyond the limits of the Local Group.

Pushing these limits further and probing the existence of IMBHs in dwarf galaxies is observationally hard. A straightforward evidence for IMBHs would be the presence of AGNs [39,49, and references therein]. One complication in the interpretation of AGN data is the possible contamination by X-ray binaries, that have a luminosity comparable to that expected from a $\sim 10^2$ – $10^3 M_{\odot}$ hole accreting from its surrounding gaseous environment.

The situation is even more complicated if we think of stellar-dynamical measurements, that exploit the dynamical signature of a Keplerian potential in the vicinity of a black hole. The radius of the sphere of influence, within which a BH dominates the gravitational potential, is $2GM_{\text{BH}}/\sigma^2$. The primary obstacle in performing measurements at the low-mass end of the BH mass function is our current inability to resolve the gravitational sphere of influence of an IMBH at distances beyond a few Mpc [9]. As an example, an IMBH of mass $M_{\text{BH}} = 10^3 M_{\odot}$ residing in a galaxy with $\sigma = 10 \text{ km s}^{-1}$ will have $r_G \approx 0.1 \text{ pc}$. Even for the most nearby dwarfs (satellites of our own Milky Way) this corresponds to sub arcsec resolution, at or below the resolution limit of existing 8-10m class telescopes. Clearly the situation only worsens if we want to probe a representative sample of nearby galaxies. At the distance (16.5 Mpc) of the Virgo Cluster — the largest collection of galaxies in the nearby universe — the resolution required to resolve $r_G \approx 0.1 \text{ pc}$ corresponds to ≈ 1 milliarcsec!

One hopes that the next generation of 25-30m optical/IR telescopes operating at their diffraction limit (~ 4 milliarcsec) can provide the first constraints on the presence of IMBHs in dwarf galaxies, but the detection of gravitational waves from a central IMBH in a dwarf galaxy undergoing a merger is possibly a

more promising probe. Dwarf galaxies have a very quiet merger history, hence we do not expect many IMBH-IMBH mergers involving dwarf galaxies at the present epoch, or in the low-redshift universe. The seed black hole mergers discussed in Section 4.1 probe a separate population of mergers, between the progenitors of galaxies which are more massive today. However, gravitational waves may also be generated in dwarf galaxies by mergers between the central IMBH and stellar remnants in the centre of the dwarf. These are analogous to the globular-cluster IMRI sources described in Section 3.1.

We can derive an estimate of the event rate based on the expected number of dwarf galaxies which can possibly host IMBHs in the interesting mass range. We may derive this number through two different methods. Firstly, we can rely on theoretical models of SMBH formation and evolution, where the seeds of MBHs are Population III remnants [105], and look for the distribution of IMBHs in dwarf galaxies. Using the dynamical model of [104], we estimate a number density of IMBHs, $n_{\text{IMBH}} \sim 0.02\text{--}0.1 \text{ Mpc}^{-3}$.

Secondly, we can ground our estimate in recent theoretical works that study the population of dwarfs as satellites of the Milky Way [85, 25, 96]. These simulations suggest that the number of satellites per halo has the following form:

$$N(> v_{\text{sat}}) = N_* \left(\frac{v_{\text{sat}}}{v_{\text{host}}} \right)^\alpha, \quad (18)$$

where v_{sat} and v_{host} are the maximum circular velocity of the satellite and the host halo, respectively. According to [25], $N_* = 0.021$ and $\alpha = -3$, while [96] find $N_* = 0.052$ and $\alpha = -3.15$. If we extrapolate the $M_{\text{BH}} - \sigma$ correlation to IMBH masses ($10^2\text{--}10^3 M_\odot$), and assume an isothermal galaxy, then $v_{\text{sat}} \sim 10\text{--}20 \text{ km s}^{-1}$. With this formalism we obtain the number of satellites in the interesting mass range per dark matter halo (N_{sat}), where the mass of the halo is uniquely determined by its maximum circular velocity. Here, we use N with appropriate subscripts to denote occupation number and n to denote number density. The number density of dark matter halos can be easily obtained by integrating the modified Press & Schechter function [93] which provides the mass function of halos, dn/dM_h . Therefore we estimate a number density of satellites (per comoving cubic Mpc) as:

$$n_{\text{sat}} = \int \frac{dn}{dM_h} N_{\text{sat}}(M_h) dM_h = 1 - 3 \text{ Mpc}^{-3}, \quad (19)$$

where the lower limit comes from [25], and the upper limit from [96]. We now have to correct for the fact that not all dwarf galaxies are likely to host an IMBH. To estimate the fraction of dwarfs that host a central IMBH, we can rely on the models described in the previous paragraph, based on [105, 104], in which a fraction $f_{\text{IMBH}} \sim 0.01\text{--}0.1$ of dwarfs host an IMBH with mass $\sim 10^2\text{--}10^3 M_\odot$. The final estimate for the number density of dwarfs hosting an IMBH is then $n_{\text{IMBH}} = f_{\text{IMBH}} n_{\text{sat}} \sim 0.01\text{--}0.3 \text{ Mpc}^{-3}$, in good agreement with the first estimate.

When we calculate the event rate of BH-IMBH mergers in dwarf galaxies, we have to further correct for the fact that only a small fraction of these tiny

satellites do indeed form stars [15, and references therein]. Based on [38], we estimate that a fraction $f_* = 0.1 - 0.2$ of dwarfs in the $v_{\text{sat}} \sim 10 - 20 \text{ km s}^{-1}$ range formed stars (which will eventually leave behind stellar mass BHs that can merge with the central IMBH). The number density of IMBHs that can be ET sources is therefore $n_{ET} = f_* n_{\text{IMBH}} \sim 0.001 - 0.06 \text{ Mpc}^{-3}$. This number density is about an order of magnitude lower than the number density of globular clusters used to normalise the rates in Section 3.1.

The capture mechanisms that seed IMRIs in dwarf galaxies are likely to be the same as those that operate in globular clusters. The event rate for the binary-hardening mechanism scales with the stellar density, n , as $n^{4/5}$, while the other mechanisms, such as direct capture, should scale approximately with n . The core stellar densities in nearby dwarf galaxies are typically much lower than in core-collapsed globular clusters, e.g., the estimate for Fornax is $\sim 10^{-1} \text{ pc}^{-3}$ [64] and for Sagittarius is $\sim 10^{-3} \text{ pc}^{-3}$ [59], compared to $\sim 10^{5.5} \text{ pc}^{-3}$ for globulars [83]. The IMRI rates for dwarf galaxies are thus likely to be orders of magnitude lower than those for globular clusters. Therefore, although it is not inconceivable that ET will detect events from dwarf galaxies, any events would be serendipitous. Moreover, there are no obvious characteristics which would allow an observer to distinguish between an event in a dwarf galaxy from one in a globular cluster based on the GW signature alone. It might be possible to make qualitative statements about dwarf galaxy IMBH populations. For instance, if ET does not detect any mergers between seed black holes at high redshift, of the type described in Section 4.1, it is very likely that BH seeds were heavy and not light. This would suggest dwarf galaxies would not contain light leftover BH seeds, and consequently that all of the observed IMRIs are occurring in globular clusters. Similarly, if seed mergers are detected but the rate of IMRIs is low or zero, it might suggest that IMBH formation in globular clusters is inefficient and any observed IMRIs are in dwarf galaxies. More refined modeling and detailed calculations are needed to understand/prove the robustness of these expectations, especially in view of the small number of seed black hole merger events and dwarf galaxy IMRIs that are predicted. In summary, while the dwarf galaxy channel should not be ignored completely, it is very unlikely to be a significant contributor to ET events or science.

5 Speculative sources

In this section we discuss some new sources and new aspects of old sources that might be explored by a future low-frequency ground-based interferometer such as ET. We examine first the possibility of observing orbiting or rotating white dwarfs near the high end of allowed masses, then discuss how the eccentricities of compact binaries could illuminate their dynamical origin.

5.1 Orbiting white dwarfs

A gravitationally bound object of average density $\bar{\rho}$ has a maximum orbital, rotational, or acoustic frequency $f_{\max} \propto (G\bar{\rho})^{1/2}$. For neutron stars this maximum is $\sim 10^3$ Hz. White dwarfs are much more extended objects, but near their maximum masses their densities are sufficient to reach $f_{\max} \sim 1$ Hz. For example, from the classic work [45], a magnesium white dwarf with maximum mass $M_{\max} = 1.363 M_{\odot}$ has a radius $R = 2.57 \times 10^{-3} R_{\odot} = 1.79 \times 10^8$ cm and therefore $(G\bar{\rho})^{1/2} = 2.7$ Hz. In the few-Hz range, therefore, one will potentially see gravitational waves from the most massive white dwarfs.

If we consider specifically such a white dwarf in a binary orbit, then the orbital frequency at the point of tidal disruption of the dwarf depends weakly on the mass of the companion. For example, suppose that the equilibrium mass and radius of the white dwarf are respectively M_{WD} and R_{WD} , and that the companion is a compact object of mass M_{comp} . When the orbital separation a is $a \sim 2R_{\text{WD}}(M_{\text{comp}}/M_{\text{WD}})^{1/3}$, tidal stripping begins [110, and others]. The orbital frequency at this point is

$$\omega = \sqrt{G(M_{\text{comp}} + M_{\text{WD}})/a^3} \sim 0.7(1 + M_{\text{WD}}/M_{\text{comp}})^{1/2}(G\bar{\rho})^{1/2}. \quad (20)$$

The gravitational wave frequency is $f_{\text{GW}} = 2f_{\text{orb}} = \omega/\pi$, implying a maximum frequency of ~ 1 Hz for comparable-mass objects such as a neutron star and a heavy white dwarf, and a maximum that is $\sim 70\%$ of this if the companion is a much more massive object such as an IMBH.

We have relatively few candidates for massive white dwarfs, hence their numbers are difficult to estimate (see [103] for a recent discussion). Models of the mass distribution suggest that perhaps $\sim 0.1 - 1\%$ of white dwarfs have masses near $M_{\text{WD}} = M_{\max}$ (e.g., see figure 10 of [21]). If we make a generous estimate that there are 10^9 double white dwarf systems in a galaxy like the Milky Way, and that $\sim 10\%$ of these have semimajor axes that allow merger by gravitational radiation within 10^{10} yr, then we expect massive white-dwarf binaries to merge at a rate per galaxy of $\sim (0.001 - 0.01)^2 \times 0.1 \times 10^9 / 10^{10} \text{ yr}^{-1} \sim 10^{-8} - 10^{-6} \text{ yr}^{-1}$. At the high end this is similar to the low end of NS-NS merger rate estimates [55]. If the ET is sensitive to such mergers out to ~ 200 Mpc, which may be optimistic given their low GW frequencies, one event per few years could be detected. Detection of these events would indicate rather precisely the maximum average density of white dwarfs, and would thus be a mechanism for establishing their mass-radius relation near the maximum mass.

5.2 Rotating hypermassive white dwarfs

Another possibility, suggested to us by [77], is that two white dwarfs with more typical masses $M_{\text{WD}} < 1 M_{\odot}$ might merge in a binary and produce a hypermassive white dwarf that spins rapidly enough that it is deformed into an ellipsoid. This is a promising candidate to explain some fraction of Type Ia supernovae [88].

To evaluate this prospect we note that if a Newtonian perfect fluid (a good model for a white dwarf) rotates uniformly then above a certain critical angular momentum L_{crit} for a given mass M the equilibrium configuration splits off from the axisymmetric Maclaurin spheroids (which emit no gravitational radiation) to the Jacobi ellipsoids. If the three axes of the ellipsoids are $a_3 \leq a_2 \leq a_1$, then according to [22, section 39] the critical angular momentum is

$$L_{\text{crit}} \approx 0.3(GM^3\bar{a})^{1/2} \quad (21)$$

where $\bar{a} \equiv (a_1 a_2 a_3)^{1/3}$. If two white dwarfs both of mass $M/2$ and radius R spiral slowly together, then their angular momentum at the point of contact is $L = \mu\sqrt{2GM\bar{R}} = \sqrt{2}/4(GM^3R)^{1/2} = 0.35(GM^3R)^{1/2}$. Since the equilibrium radius of the hypermassive object is smaller than the radii of the original white dwarfs, the angular momentum is sufficient to produce an ellipsoidal figure. Again from [22, section 39], the angular velocity of this configuration will be $\Omega \approx (G\bar{\rho})^{1/2}$ and hence the dominant gravitational wave frequency will be $f_{\text{GW}} \approx (G\bar{\rho})^{1/2}/\pi$.

The amplitude of gravitational waves depends on the ellipticity $\epsilon \equiv (I_1 - I_2)/I_3$, where I indicates the moment of inertia and the number corresponds to the axis. Near the critical angular momentum, slight changes in L produce large changes in ϵ , and ϵ of several tenths is possible. If we scale the moment of inertia I_3 to 10^{49} g cm^2 (roughly appropriate for $M = 1.4 M_\odot$ and $R = 10^8 \text{ cm}$) then the strain amplitude at a distance r is

$$h \approx 10^{-26} \left(\frac{\epsilon}{0.1} \right) \left(\frac{I_3}{10^{49} \text{ g cm}^2} \right) \left(\frac{100 \text{ Mpc}}{r} \right) \left(\frac{f_{\text{GW}}}{1 \text{ Hz}} \right). \quad (22)$$

Gravitational waves remove rotational energy from the star, such that

$$\dot{\omega} = -\frac{32}{5} \frac{G}{c^5} \epsilon^2 I_3 \omega^5 \quad (23)$$

where $\omega = \pi f_{\text{GW}}$. As a result, the characteristic spindown time is

$$T_{\text{spindown}} = \omega/|\dot{\omega}| \approx 200 \text{ yr} \left(\frac{0.1}{\epsilon} \right)^2 \left(\frac{10^{49} \text{ g cm}^2}{I_3} \right) \left(\frac{f_{\text{GW}}}{1 \text{ Hz}} \right)^{-4}. \quad (24)$$

Thus the frequency will be stable for long enough that integration over weeks to months may be practical, partially offsetting the low expected amplitudes.

Type Ia supernovae are estimated to occur once per 1000 years in galaxies such as the Milky Way [88], so even if only 10% of SNe Ia are binary mergers, the overall astrophysical rate is competitive with double neutron star mergers. Even though the ET sensitivity to gravitational waves from these binary white dwarf mergers will be much lower than for double neutron star mergers, the detection of gravitational waves from any such event may provide a new view on these important supernovae.

5.3 Eccentric binaries

In the sensitivity bands of second-generation gravitational wave detectors such as Advanced LIGO and Advanced Virgo, most compact binaries will be very close to circular. (For a proposed scenario where this may not be true, see [75]; another possibility includes direct captures of compact objects by IMBHs as precursors to eccentric IMRIs in globular clusters, although this formation mechanism is uncommon relative to the one described in Section 3.1, which will produce circular IMRIs). This is because for moderate to high eccentricities, gravitational radiation essentially reduces the semimajor axis of a binary while keeping the pericenter fixed. Therefore, to have palpable eccentricity at a given frequency, the pericenter at formation or at the last dynamical interaction must be inside the radius of a circular orbit at that frequency. For example, a binary of two $1.4 M_{\odot}$ neutron stars must have a pericenter less than 700 km to be significantly eccentric at a gravitational wave frequency $f_{\text{GW}} = 2f_{\text{orb}} = 10$ Hz. This is highly improbable for a field binary, and is even difficult to arrange for binary-single scattering in dense stellar environments.

Somewhat higher eccentricities can be obtained via the Kozai secular resonance [56]. As explored in the context of black holes by [68, 109] a binary-binary interaction can result in a stable hierarchical triple in some tens of percent of encounters. If the inner binary and the outer tertiary have orbital planes that are inclined significantly with respect to each other, then over many orbital periods the inclination and eccentricity of the inner binary change periodically, leading at points in the cycle to very small pericenters and thus potentially observable eccentricity after the gravitational-wave driven inspiral. The eccentricity at 40 Hz is almost always very small (below 0.1), but at 10 Hz there are a few orientations in which the eccentricity can be a few tenths [109]. At still lower frequencies the eccentricity will be yet higher, because for low eccentricities e , $e \propto f^{-19/18}$.

This implies that detector sensitivity at low frequencies will be important to determine the origin of compact binaries. In-situ formation from a massive main-sequence binary is still highly unlikely to produce detectable eccentricities: in order to have eccentricity at 1 Hz, the pericenter distance would have to be $\lesssim 3000$ km immediately after the second supernova. In contrast, dynamical effects such as the Kozai resonance are expected to produce eccentric orbits at a few Hz. As a result, observation of a few BH-BH or BH-NS inspirals at a few Hz will illuminate their formation processes in a way that is not as easy at higher frequencies.

6 Summary and Discussion

We have discussed gravitational waves generated by intermediate-mass black holes as possible sources for the Einstein Telescope. Intermediate-mass black holes may be formed via two alternative channels — (i) they may be formed in the early Universe if MBH seeds are light (seed IMBH); (ii) they may form

in globular clusters via runaway collisions between stars (cluster IMBH). In both cases, there are two distinct types of system that might be sources of gravitational waves for ET — (a) mergers between binaries containing two IMBHs; (b) mergers of stellar remnants with IMBHs (IMRIs).

Mergers between seed IMBHs occur following galaxy mergers during the hierarchical assembly of structure. ET will detect a few to a few tens of seed black hole merger events over three years at redshifts as high as $z \sim 8-10$. An ET network would in addition be able to determine the luminosity distance to these events to an accuracy $\sim 30\%$, which would be sufficient to say confidently that an event involves *intermediate-mass* black holes and is occurring at *high redshift*. IMRIs involving seed IMBHs could occur in dwarf galaxies, but the event rate is likely to be very low, which makes it unlikely that this will be a significant contributor to the ET event rate. Binary IMBHs in globular clusters might be detected by ET at a rate of $\sim 2000 \frac{g}{0.1} \frac{g_{cl}}{0.1}$ per year, where g is the fraction of globular clusters that produce IMBH-IMBH binaries and g_{cl} is the fraction of total star formation that occurs in globular clusters with masses $5 \times 10^4 \leq M_{cl}/M_{\odot} \leq 10^7$. Core-collapsed globular clusters are also a more promising host for IMRIs detectable by ET. The IMRI event rate for ET could be range up to several hundred per year. However, there are significant uncertainties, not least of which is whether IMBHs form at all in the stellar environments of globular clusters.

We have also discussed several speculative sources, the detection of which is made possible by the improved sensitivity of ET at low frequency. High-mass white dwarfs can survive tidal disruption long enough to reach orbital frequencies $f_{\max} \sim 1\text{Hz}$ in binaries. If such systems are detected near the lower frequency cut-off of ET, this will yield constraints on the maximum densities that white dwarfs can reach. Hypermassive white dwarfs formed by the mergers of normal white dwarfs in binaries could also be sources for gravitational waves at frequencies around 1Hz as they will be rapidly rotating and can support relatively significant ellipticities. Such systems could be associated with a fraction of unusual Type Ia supernovae. Finally, dynamical processes such as the Kozai mechanism can excite significant eccentricity in BH-BH and BH-NS binaries. While the majority of these systems will have circularized by the time they enter the sensitivity range of Advanced LIGO, they could still have significant residual eccentricity when their orbital frequency is in the 1–10Hz range, which ET will probe. ET detections of significant numbers of eccentric binaries at low-frequency will be an indicator of the efficiency of dynamical formation mechanisms.

ET detections of these systems will yield important science products. The very existence of BHs in the $100-1000M_{\odot}$ range is uncertain, so a single robust detection of an IMBH by ET will be of huge significance. If ET detects any seed black hole mergers at high redshift, it will be strong evidence that black hole seeds were *light*, which will help discriminate between light and heavy seed scenarios for the growth of structure in the Universe. Observations of mergers between more massive black holes with LISA do not have the same discriminating power, as they cannot distinguish between $\sim 10^5 M_{\odot}$ MBHs

that formed through direct collapse or the collapse of a massive Pop III star and those that formed through a sequence of mergers [92,34]. A significant number of ET detections of seed black hole mergers may provide constraints on the mass distribution of black hole seeds, and their early accretion history. Detection of a significant number of IMRIs with ET will indicate that IMBHs form readily in globular clusters (since the rate of IMRIs in dwarf galaxies is so low). The characteristics of the IMRI events will provide constraints on the astrophysics of dense stellar environments, and on the efficiency of capture processes operating within them. ET detections of white dwarfs undergoing tidal disruption will provide important constraints on the physics of degenerate matter, including the maximum density and mass that white dwarfs can reach. Detections of rotating hypermassive white dwarfs would provide information about channels leading to supernovae, while detections of a significant population of eccentric coalescing binaries will shed light on the mechanisms leading to their formation.

In addition to these astrophysical pay-offs, ET IMRI sources can be used for testing aspects of relativity theory, in particular verifying that the central object is indeed a black hole as described by the Kerr metric of general relativity. This has been explored extensively in the context of extreme-mass-ratio inspiral events detectable by LISA (see, for example, [6] and references therein). In the course of such an inspiral, the orbit of the smaller object traces out the spacetime geometry of the large body and hence the emitted gravitational waves encode a map of the spacetime structure. One way to characterize this is in terms of the multipole moments of the spacetime. It was demonstrated by Ryan [89], for nearly circular and nearly equatorial orbits, that successive multipole moments of an arbitrary spacetime are encoded at different orders in an expansion of the orbital precession frequencies as functions of the azimuthal orbital frequency. Since these frequencies can be measured from the emitted gravitational waves, a multipole map of the spacetime can in principle be measured. Similar multipole measurements are also possible from observations of ringdown radiation following mergers [14]. For a Kerr black hole, the mass M and angular momentum S determine all higher-order mass, M_l , and current, S_l , multipole moments of the spacetime:

$$M_l + iS_l = M(iS/M)^l. \quad (25)$$

Measuring just three multipole moments and finding them to be inconsistent with this formula is therefore enough to demonstrate that the central object is not a Kerr black hole. For IMRIs, it has been shown that Advanced LIGO could measure an $O(1)$ fractional deviation in the mass quadrupole moment, M_2 , for typical systems [18]. These results have not been generalised to ET as yet. However, ET will improve this significantly for two reasons — (i) the SNR of a source at fixed distance will increase by a factor of 10 or more; and (ii) ET will observe the sources at lower frequencies. The ability to measure multipole moments improves significantly with the number of gravitational-wave cycles observed. At the leading-order Newtonian approximation, a $1M_\odot + 100M_\odot$ system has ~ 500 cycles remaining until plunge when the frequency is 10Hz,

but this increases to ~ 1500 for a frequency of 5Hz, ~ 4000 for 3Hz and ~ 25000 for a frequency of 1Hz [29]. ET should thus be able to carry out tests of the Kerr nature of the central object that are significantly better than those possible with LIGO. Further research is required to quantify the improvement that will be possible, and how this will compare to the results from LISA EMRI events.

There are various uncertainties which may affect the scientific impact of the ET measurements discussed here. One important consideration is how to distinguish between IMBH events that arise from seed black holes and those that arise from IMBHs formed in globular clusters. Using ET measurements to constrain hierarchical structure formation relies on identification of mergers as seed black hole mergers, but as we have seen, there may also be IMBH binary mergers in globular clusters. The masses and redshifts of the events may provide a robust discriminator, but more work is needed to understand if this is indeed the case, or whether other characteristic features exist that we can exploit.

The eventual sensitivity that is achieved by ET also has bearing on these results. The speculative sources that were discussed in Section 5 all rely on ET having sensitivity in the 1–10Hz band, and low-frequency sensitivity also improves the accuracy of the tests of relativity using IMRIs. ET may only reach a low frequency sensitivity of ~ 3 Hz, which would have an impact on all of this science and perhaps eliminate the possibility of detecting gravitational radiation from massive white dwarfs. This should be explored further in the future.

Finally, there are data-analysis concerns. The ET data stream will be very source-rich, and so the identification of individual sources of different types in the presence of this confusion will be a challenging problem. For instance, neutron star binary systems will create a confusion background near 1Hz [87]. The data-analysis challenges for ET will inevitably change the SNRs required for detection of individual sources, and the accuracy with which source parameters can be estimated. This will change the rate predictions, but the uncertainties due to data analysis are likely small compared to the underlying uncertainties in the astrophysics.

Acknowledgments

JG’s work is supported by a Royal Society University Research Fellowship. IM and MV acknowledge support from NASA ATP Grant NNX07AH22G. MCM acknowledges NASA ATP grant NNX08AH29G.

References

1. T. Abel, G. L. Bryan, and M. L. Norman, *The Formation of the First Star in the Universe*, *Science* **295** (2002), 93–98.

2. F. Acernese et al., *Status of Virgo*, *Classical and Quantum Gravity* **25** (2008), no. 11, 114045–+.
3. P. Ajith, *Gravitational-wave data analysis using binary black-hole waveforms*, *Classical and Quantum Gravity* **25** (2008), no. 11, 114033–+.
4. P. Ajith, S. Babak, Y. Chen, M. Hewitson, B. Krishnan, A. M. Sintes, J. T. Whelan, B. Brüggmann, P. Diener, N. Dorband, J. Gonzalez, M. Hannam, S. Husa, D. Pollney, L. Rezzolla, L. Santamaría, U. Sperhake, and J. Thornburg, *Template bank for gravitational waveforms from coalescing binary black holes: Nonspinning binaries*, *Phys. Rev. D* **77** (2008), no. 10, 104017–+.
5. P. Amaro-Seoane and M. Freitag, *Intermediate-Mass Black Holes in Colliding Clusters: Implications for Lower Frequency Gravitational-Wave Astronomy*, *Astrophysical Journal Letters* **653** (2006), L53–L56.
6. P. Amaro-Seoane, J. R. Gair, M. Freitag, M. C. Miller, I. Mandel, C. J. Cutler, and S. Babak, *Intermediate and extreme mass-ratio inspirals – astrophysics, science applications and detection using LISA*, *Classical and Quantum Gravity* **24** (2007), 113–+.
7. L. Barack and N. Sago, *Gravitational self-force on a particle in circular orbit around a Schwarzschild black hole*, *Phys. Rev. D* **75** (2007), no. 6, 064021–+.
8. ———, *Gravitational Self-Force Correction to the Innermost Stable Circular Orbit of a Schwarzschild Black Hole*, *Physical Review Letters* **102** (2009), no. 19, 191101–+.
9. A. Barth, P. Cote, M. Milosavljevic, A. Seth, R. van der Marel, and M. Volonteri, *The Nuclei of Low-Mass Galaxies and the Search for the Smallest Massive Black Holes*, *Astronomy* **2010** (2009), 12–+.
10. A. J. Barth, L. C. Ho, R. E. Rutledge, and W. L. W. Sargent, *POX 52: A Dwarf Seyfert 1 Galaxy with an Intermediate-Mass Black Hole*, *ApJ* **607** (2004), 90–102.
11. M. C. Begelman, M. Volonteri, and M. J. Rees, *Formation of supermassive black holes by direct collapse in pre-galactic haloes*, *MNRAS* **370** (2006), 289–298.
12. P.L. Bender et al., *Lisa pre-phase a report; second edition*, Tech. Report MPQ233, 1998.
13. C. T. Berghea, K. A. Weaver, E. J. M. Colbert, and T. P. Roberts, *Testing the Paradigm that Ultraluminous X-ray Sources as a Class Represent Accreting Intermediate-Mass Black Holes*, *ArXiv e-prints* (2008), 0807.1547.
14. E. Berti, V. Cardoso, and C. M. Will, *Gravitational-wave spectroscopy of massive black holes with the space interferometer LISA*, *Phys. Rev. D* **73** (2006), no. 6, 064030–+.
15. M. S. Bovill and M. Ricotti, *Pre-Reionization Fossils, Ultra-Faint Dwarfs, and the Missing Galactic Satellite Problem*, *Astrophysical Journal* **693** (2009), 1859–1870.
16. V. Bromm, P. S. Coppi, and R. B. Larson, *Forming the First Stars in the Universe: The Fragmentation of Primordial Gas*, *ApJL* **527** (1999), L5–L8.
17. V. Bromm and A. Loeb, *Formation of the First Supermassive Black Holes*, *ApJ* **596** (2003), 34–46.
18. D. A. Brown, J. Brink, H. Fang, J. R. Gair, C. Li, G. Lovelace, I. Mandel, and K. S. Thorne, *Prospects for Detection of Gravitational Waves from Intermediate-Mass-Ratio Inspirals*, *Physical Review Letters* **99** (2007), no. 20, 201102–+.
19. A. Buonanno, Y. Pan, J. G. Baker, J. Centrella, B. J. Kelly, S. T. McWilliams, and J. R. van Meter, *Approaching faithful templates for nonspinning binary black holes using the effective-one-body approach*, *Phys. Rev. D* **76** (2007), no. 10, 104049–+.
20. A. Buonanno, Y. Pan, H. P. Pfeiffer, M. A. Scheel, L. T. Buchman, and L. E. Kidder, *Effective-one-body waveforms calibrated to numerical relativity simulations: Coalescence of nonspinning, equal-mass black holes*, *Phys. Rev. D* **79** (2009), no. 12, 124028–+.
21. S. Catalán, J. Isern, E. García-Berro, and I. Ribas, *The initial-final mass relationship of white dwarfs revisited: effect on the luminosity function and mass distribution*, *MNRAS* **387** (2008), 1693–1706.
22. S. Chandrasekhar, *Ellipsoidal figures of equilibrium: The Silliman Foundation Lectures*, Yale University Press, New Haven, 1969.
23. C. Cutler and M. Vallisneri, *LISA detections of massive black hole inspirals: Parameter extraction errors due to inaccurate template waveforms*, *Phys. Rev. D* **76** (2007), no. 10, 104018–+.
24. B. Devecchi and M. Volonteri, *Formation of the First Nuclear Clusters and Massive Black Holes at High Redshift*, *Astrophysical Journal* **694** (2009), 302–313.

25. J. Diemand, M. Kuhlen, and P. Madau, *Formation and Evolution of Galaxy Dark Matter Halos and Their Substructure*, *Astrophysical Journal* **667** (2007), 859–877.
26. L. Ferrarese and H. Ford, *Supermassive Black Holes in Galactic Nuclei: Past, Present and Future Research*, *Space Science Reviews* **116** (2005), 523–624.
27. L. Ferrarese and D. Merritt, *A Fundamental Relation between Supermassive Black Holes and Their Host Galaxies*, *ApJ* **539** (2000), L9–L12.
28. L. S. Finn and D. F. Chernoff, *Observing binary inspiral in gravitational radiation: One interferometer*, *Phys. Rev. D* **47** (1993), 2198–2219.
29. Lee Samuel Finn and Kip S. Thorne, *Gravitational waves from a compact star in a circular, inspiral orbit, in the equatorial plane of a massive, spinning black hole, as observed by lisa*, *Phys. Rev. D* **62** (2000), 124021.
30. J. M. Fregeau, S. L. Larson, M. C. Miller, R. O’Shaughnessy, and F. A. Rasio, *Observing IMBH-IMBH Binary Coalescences via Gravitational Radiation*, *Astrophysical Journal Letters* **646** (2006), L135–L138.
31. A. Freise, S. Chelkowski, S. Hild, W. Del Pozzo, A. Perreca, and A. Vecchio, *Triple Michelson interferometer for a third-generation gravitational wave detector*, *Classical and Quantum Gravity* **26** (2009), no. 8, 085012+.
32. C. L. Fryer, S. E. Woosley, and A. Heger, *Pair-Instability Supernovae, Gravity Waves, and Gamma-Ray Transients*, *ApJ* **550** (2001), 372–382.
33. J. R. Gair, *Probing black holes at low redshift using LISA EMRI observations*, *Classical and Quantum Gravity* **26** (2009), no. 9, 094034+.
34. J. R. Gair, I. Mandel, A. Sesana, and A. Vecchio, *Probing seed black holes using future gravitational-wave detectors*, *ArXiv e-prints* (2009), 0907.3292.
35. K. Gebhardt, R. Bender, G. Bower, A. Dressler, S. M. Faber, A. V. Filippenko, R. Green, C. Grillmair, L. C. Ho, J. Kormendy, T. R. Lauer, J. Magorrian, J. Pinkney, D. Richstone, and S. Tremaine, *A Relationship between Nuclear Black Hole Mass and Galaxy Velocity Dispersion*, *ApJ* **539** (2000), L13–L16.
36. K. Gebhardt, T. R. Lauer, J. Kormendy, J. Pinkney, G. A. Bower, R. Green, T. Gull, J. B. Hutchings, M. E. Kaiser, C. H. Nelson, D. Richstone, and D. Weistrop, *M33: A Galaxy with No Supermassive Black Hole*, *Astronomical Journal* **122** (2001), 2469–2476.
37. E. Glebbeek, E. Gaburov, S. E. de Mink, O. R. Pols, and S. F. Portegies Zwart, *The evolution of runaway stellar collision products*, *A&A* **497** (2009), 255–264.
38. N. Y. Gnedin and A. V. Kravtsov, *Fossils of Reionization in the Local Group*, *Astrophysical Journal* **645** (2006), 1054–1061.
39. J. E. Greene and L. C. Ho, *The Mass Function of Active Black Holes in the Local Universe*, *Astrophysical Journal* **667** (2007), 131–148.
40. H. Grote and the LIGO Scientific Collaboration, *The status of GEO 600*, *Classical and Quantum Gravity* **25** (2008), no. 11, 114043+.
41. K. Gültekin, M. C. Miller, and D. P. Hamilton, *Growth of Intermediate-Mass Black Holes in Globular Clusters*, *Astrophysical Journal* **616** (2004), 221–230.
42. ———, *Three-Body Dynamics with Gravitational Wave Emission*, *Astrophysical Journal* **640** (2006), 156–166.
43. M. A. Gürkan, J. M. Fregeau, and F. A. Rasio, *Massive Black Hole Binaries from Collisional Runaways*, *Astrophysical Journal* **640** (2006), L39–L42.
44. M. A. Gürkan, M. Freitag, and F. A. Rasio, *Formation of Massive Black Holes in Dense Star Clusters. I. Mass Segregation and Core Collapse*, *Astrophysical Journal* **604** (2004), 632–652.
45. T. Hamada and E. E. Salpeter, *Models for Zero-Temperature Stars.*, *Astrophysical Journal* **134** (1961), 683+.
46. N. Häring and H.-W. Rix, *On the Black Hole Mass-Bulge Mass Relation*, *Astrophysical Journal* **604** (2004), L89–L92.
47. S. Hild, S. Chelkowski, and A. Freise, *Pushing towards the ET sensitivity using ‘conventional’ technology*, *ArXiv e-prints* (2008), 0810.0604.
48. S. Hild, S. Chelkowski, A. Freise, J. Franc, N. Morgado, R. Flaminio, and R. DeSalvo, *A Xylophone Configuration for a third Generation Gravitational Wave Detector*, *ArXiv e-prints* (2009), 0906.2655.
49. L. C. Ho, *Nuclear Activity in Nearby Galaxies*, *ARA&A* **46** (2008), 475–539.

-
50. D. W. Hogg, *Distance measures in cosmology*, ArXiv Astrophysics e-prints (1999), astro-ph/9905116.
 51. C. Hopman, private communication, 2007.
 52. E. A. Huerta and J. R. Gair, *Influence of conservative corrections on parameter estimation for extreme-mass-ratio inspirals*, Phys. Rev. D **79** (2009), no. 8, 084021–+.
 53. J. R. Hurley, *Ratios of star cluster core and half-mass radii: a cautionary note on intermediate-mass black holes in star clusters*, MNRAS **379** (2007), 93–99.
 54. N. Ivanova, K. Belczynski, J. M. Fregeau, and F. A. Rasio, *The evolution of binary fractions in globular clusters*, MNRAS **358** (2005), 572–584.
 55. V. Kalogera, K. Belczynski, C. Kim, R. O’Shaughnessy, and B. Willems, *Formation of double compact objects*, Physics Reports **442** (2007), 75–108.
 56. Y. Kozai, *Secular perturbations of asteroids with high inclination and eccentricity*, Astronomical Journal **67** (1962), 591–+.
 57. P. Madau and M. J. Rees, *Massive Black Holes as Population III Remnants*, ApJL **551** (2001), L27–L30.
 58. J. Magorrian, S. Tremaine, D. Richstone, R. Bender, G. Bower, A. Dressler, S. M. Faber, K. Gebhardt, R. Green, C. Grillmair, J. Kormendy, and T. Lauer, *The Demography of Massive Dark Objects in Galaxy Centers*, AJ **115** (1998), 2285–2305.
 59. S. R. Majewski, P. M. Frinchaboy, W. E. Kunkel, R. Link, R. R. Muñoz, J. C. Osthheimer, C. Palma, R. J. Patterson, and D. Geisler, *Exploring Halo Substructure with Giant Stars. VI. Extended Distributions of Giant Stars around the Carina Dwarf Spheroidal Galaxy: How Reliable Are They?*, Astronomical Journal **130** (2005), 2677–2700.
 60. R. K. Malbon, C. M. Baugh, C. S. Frenk, and C. G. Lacey, *Black hole growth in hierarchical galaxy formation*, MNRAS **382** (2007), 1394–1414.
 61. I. Mandel, *Spin distribution following minor mergers and the effect of spin on the detection range for low-mass-ratio inspirals*, ArXiv e-prints (2007), 0707.0711.
 62. I. Mandel, D. A. Brown, J. R. Gair, and M. C. Miller, *Rates and Characteristics of Intermediate Mass Ratio Inspirals Detectable by Advanced LIGO*, Astrophysical Journal **681** (2008), 1431–1447.
 63. I. Mandel and J. R. Gair, *Can we detect intermediate mass ratio inspirals?*, Classical and Quantum Gravity **26** (2009), no. 9, 094036–+.
 64. Mario Mateo, *Dwarf galaxies of the local group*, Annu. Rev. Astron. Astrophys. **36** (1998), 435–506.
 65. D. Merritt, L. Ferrarese, and C. L. Joseph, *No Supermassive Black Hole in M33?*, Science **293** (2001), 1116–1119.
 66. M. C. Miller, *Intermediate-Mass Black Holes as LISA Sources*, ArXiv e-prints (2008), 0812.3028.
 67. M. C. Miller and E. J. M. Colbert, *Intermediate-Mass Black Holes*, International Journal of Modern Physics D **13** (2004), 1–64.
 68. M. C. Miller and D. P. Hamilton, *Four-Body Effects in Globular Cluster Black Hole Coalescence*, Astrophysical Journal **576** (2002), 894–898.
 69. ———, *Production of intermediate-mass black holes in globular clusters*, MNRAS **330** (2002), 232–240.
 70. M. Milosavljević, S. M. Couch, and V. Bromm, *Accretion Onto Intermediate-Mass Black Holes in Dense Protogalactic Clouds*, Astrophysical Journal **696** (2009), L146–L149.
 71. H. Mouri and Y. Taniguchi, *Mass Segregation in Star Clusters: Analytic Estimation of the Timescale*, Astrophysical Journal **580** (2002), 844–849.
 72. ———, *Runaway Merging of Black Holes: Analytical Constraint on the Timescale*, Astrophysical Journal **566** (2002), L17–L20.
 73. F. Nakamura and M. Umemura, *On the Initial Mass Function of Population III Stars*, ApJ **548** (2001), 19–32.
 74. E. Noyola, K. Gebhardt, and M. Bergmann, *Gemini and Hubble Space Telescope Evidence for an Intermediate-Mass Black Hole in ω Centauri*, Astrophysical Journal **676** (2008), 1008–1015.
 75. R. M. O’Leary, B. Kocsis, and A. Loeb, *Gravitational waves from scattering of stellar-mass black holes in galactic nuclei*, MNRAS **395** (2009), 2127–2146.

76. R. M. O’Leary, F. A. Rasio, J. M. Fregeau, N. Ivanova, and R. O’Shaughnessy, *Binary Mergers and Growth of Black Holes in Dense Star Clusters*, *Astrophysical Journal* **637** (2006), 937–951.
77. C. Ott, private communication, 2009.
78. P. C. Peters, *Gravitational radiation and the motion of two point masses*, *Phys. Rev.* **136** (1964), B1224.
79. E. Poisson, *The Motion of Point Particles in Curved Spacetime*, *Living Reviews in Relativity* **7** (2004), 6–+.
80. S. F. Portegies Zwart, H. Baumgardt, P. Hut, J. Makino, and S. L. W. McMillan, *Formation of massive black holes through runaway collisions in dense young star clusters*, *Nature* **428** (2004), 724–726.
81. S. F. Portegies Zwart and S. L. W. McMillan, *Black hole mergers in the universe*, *Astrophysical Journal* **528** (2000), L17.
82. W. H. Press and P. Schechter, *Formation of Galaxies and Clusters of Galaxies by Self-Similar Gravitational Condensation*, *Astrophysical Journal* **187** (1974), 425–438.
83. C. Pryor and G. Meylan, *Velocity Dispersions for Galactic Globular Clusters*, *Structure and Dynamics of Globular Clusters* (S. G. Djorgovski and G. Meylan, eds.), *Astronomical Society of the Pacific Conference Series*, vol. 50, January 1993, pp. 357–+.
84. G. D. Quinlan, *The dynamical evolution of massive black hole binaries I. Hardening in a fixed stellar background*, *New Astronomy* **1** (1996), 35–56.
85. D. Reed, F. Governato, T. Quinn, J. Gardner, J. Stadel, and G. Lake, *Dark matter subhaloes in numerical simulations*, *MNRAS* **359** (2005), 1537–1548.
86. M. J. Rees, *Emission from the nuclei of nearby galaxies - Evidence for massive black holes*, *Structure and Properties of Nearby Galaxies* (E. M. Berkhuijsen and R. Wielebinski, eds.), *IAU Symposium*, vol. 77, 1978, pp. 237–242.
87. T. Regimbau and S. A. Hughes, *Gravitational-wave confusion background from cosmological compact binaries: Implications for future terrestrial detectors*, *Phys. Rev. D* **79** (2009), no. 6, 062002–+.
88. A. J. Ruiter, K. Belczynski, and C. Fryer, *Rates and Delay Times of Type Ia Supernovae*, *Astrophysical Journal* **699** (2009), 2026–2036.
89. F. D. Ryan, *Gravitational waves from the inspiral of a compact object into a massive, axisymmetric body with arbitrary multipole moments*, *Phys. Rev.* **D52** (1995), 5707–5718.
90. A. Sesana, J. Gair, I. Mandel, and A. Vecchio, *Observing Gravitational Waves from the First Generation of Black Holes*, *Astrophysical Journal* **698** (2009), L129–L132.
91. A. Sesana, F. Haardt, P. Madau, and M. Volonteri, *Low-Frequency Gravitational Radiation from Coalescing Massive Black Hole Binaries in Hierarchical Cosmologies*, *Astrophysical Journal* **611** (2004), 623–632.
92. A. Sesana, M. Volonteri, and F. Haardt, *The imprint of massive black hole formation models on the LISA data stream*, *MNRAS* **377** (2007), 1711–1716.
93. R. K. Sheth and G. Tormen, *Large-scale bias and the peak background split*, *MNRAS* **308** (1999), 119–126.
94. D. Sigg and the LIGO Scientific Collaboration, *Status of the LIGO detectors*, *Classical and Quantum Gravity* **25** (2008), no. 11, 114041–+.
95. M. Spaans and J. Silk, *Pregalactic Black Hole Formation with an Atomic Hydrogen Equation of State*, *Astrophysical Journal* **652** (2006), 902–906.
96. V. Springel, J. Wang, M. Vogelsberger, A. Ludlow, A. Jenkins, A. Helmi, J. F. Navarro, C. S. Frenk, and S. D. M. White, *The Aquarius Project: the subhaloes of galactic haloes*, *MNRAS* **391** (2008), 1685–1711.
97. C. C. Steidel, K. L. Adelberger, M. Giavalisco, M. Dickinson, and M. Pettini, *Lyman-Break Galaxies at $z \approx 4$ and the Evolution of the Ultraviolet Luminosity Density at High Redshift*, *Astrophysical Journal* **519** (1999), 1–17.
98. Y. Taniguchi, Y. Shioya, T. G. Tsuru, and S. Ikeuchi, *Formation of Intermediate-Mass Black Holes in Circumnuclear Regions of Galaxies*, *PASJ* **52** (2000), 533–537.
99. M. Trenti, *Dynamical evidence for intermediate mass black holes in old globular clusters*, *ArXiv Astrophysics e-prints* (2006), arXiv:astro-ph/0612040.
100. M. Vallisneri, *Use and abuse of the Fisher information matrix in the assessment of gravitational-wave parameter-estimation prospects*, *Phys. Rev. D* **77** (2008), no. 4, 042001–+.

-
101. M. Valluri, L. Ferrarese, D. Merritt, and C. L. Joseph, *The Low End of the Supermassive Black Hole Mass Function: Constraining the Mass of a Nuclear Black Hole in NGC 205 via Stellar Kinematics*, *Astrophysical Journal* **628** (2005), 137–152.
 102. M. van der Sluys, I. Mandel, V. Raymond, V. Kalogera, C. Roever, and N. Christensen, *Parameter estimation for signals from compact binary inspirals injected into LIGO data*, *ArXiv e-prints* (2009), 0905.1323.
 103. S. Vennes and A. Kawka, *On the empirical evidence for the existence of ultramassive white dwarfs*, *MNRAS* **389** (2008), 1367–1374.
 104. M. Volonteri, F. Haardt, and K. Gültekin, *Compact massive objects in Virgo galaxies: the black hole population*, *MNRAS* **384** (2008), 1387–1392.
 105. M. Volonteri, F. Haardt, and P. Madau, *The Assembly and Merging History of Supermassive Black Holes in Hierarchical Models of Galaxy Formation*, *ApJ* **582** (2003), 559–573.
 106. M. Volonteri, G. Lodato, and P. Natarajan, *The evolution of massive black hole seeds*, *MNRAS* **383** (2008), 1079–1088.
 107. M. Volonteri, R. Salvaterra, and F. Haardt, *Constraints on the accretion history of massive black holes from faint X-ray counts*, *MNRAS* **373** (2006), 121–127.
 108. M. G. Walker, M. Mateo, and E. W. Olszewski, *Stellar Velocities in the Carina, Fornax, Sculptor, and Sextans dSph Galaxies: Data From the Magellan/MMFS Survey*, *Astronomical Journal* **137** (2009), 3100–3108.
 109. L. Wen, *On the Eccentricity Distribution of Coalescing Black Hole Binaries Driven by the Kozai Mechanism in Globular Clusters*, *Astrophysical Journal* **598** (2003), 419–430.
 110. P. Wiggins and D. Lai, *Tidal Interaction between a Fluid Star and a Kerr Black Hole in Circular Orbit*, *Astrophysical Journal* **532** (2000), 530–539.
 111. N. Yoshida, K. Omukai, L. Hernquist, and T. Abel, *Formation of Primordial Stars in a Λ CDM Universe*, *Astrophysical Journal* **652** (2006), 6–25.
 112. L. R. Yungelson, E. P. J. van den Heuvel, J. S. Vink, S. F. Portegies Zwart, and A. de Koter, *On the evolution and fate of super-massive stars*, *A&A* **477** (2008), 223–237.